A Fast 3D Full-Wave Solver for Nanophotonics

by

Lei Zhang

B.Eng., Electrical Engineering
University of Science and Technology of China (2003)
M.Eng., Electrical Engineering
National University of Singapore (2005)

Submitted to the School of Engineering
in partial fulfillment of the requirements for the degree of

Master of Science in Computation for Design and Optimization

at the

MASSACHUSETTS INSTITUTE OF TECHNOLOGY

June 2007

Author .....
School of Engineering
May 11, 2007

Certified by .....
Jacob K. White
Professor of Electrical Engineering
Thesis Supervisor

Accepted by .....
Jaime Peraire
Professor of Aeronautics and Astronautics
Co-Director, Computation for Design and Optimization Program

A Fast 3D Full-Wave Solver for Nanophotonics

by

Lei Zhang

Submitted to the School of Engineering
on May 11, 2007, in partial fulfillment of the
requirements for the degree of
Master of Science in Computation for Design and Optimization

Abstract

Conventional fast integral equation solvers seem to be ideal approaches for simulating 3-D nanophotonic devices, as these devices are considered to be open structures, generating fields in both an interior channel and in the infinite exterior domain. However, many devices of interest, such as optical ring resonator filters or waveguides, have channels that can not be terminated without generating numerical reflections. Therefore, designing absorbers for these channels is a new problem for integral equation methods, as integral equation methods were initially developed for problems with finite surfaces. In this thesis we present a technique to eliminate reflections, making the channel volume conductive outside the domain of interest. The surface integral equation (SIE) method is employed to take advantage of the piecewise homogeneous medium. The Poggio-Miller-Chang-Harrington-Wu (PMCHW) formulation is formed and the boundary element method is employed to construct and solve a linear system. Moreover, the block Toeplitz matrix property and using FFT helps reduce memory requirement, and accelerate the circulant matrix vector product. Numerical experiments are presented to demonstrate that this method can effectively reduce reflections to 1%, and is easily incorporated in an fast integral equation solver.

Thesis Supervisor: Jacob K. White
Title: Professor of Electrical Engineering

Acknowledgments

I would like to take this chance to thank my advisor Professor Jacob K. White. Great appreciation goes to his helpful discussion, smart ideas, and strong supports. I also want to thank Professor Steven G. Johnson in Math department, who will be co-supervisor for my PhD thesis. He teaches me electromagnetics from a physicist's point of view, and has numerous fresh ideas.

Meanwhile, I would like to thank my collaborator Jung Hoon Lee, a mathematician and perfectionist. For the past two years, he has been offering me numerous help and wonderful discussion, and provides a beautiful integral equation code and an efficient numerical panel integration package. He is smart and stubborn, so that I have seldom won our debates. I also wanted to thank Steve Leibman, a talented programmer and fast learner. He is the first patient reader of this thesis, and gave me very helpful comments and grammar corrections. Many thanks also goes to my awesome officemates, Kin Cheong Sou, a genius mathematician and optimization expert, and Bo Kim, a linguist and computational biologist. I also wanted to thank Professor Luca Daniel and all other my groupmates, Brad Bond, Dmitry Vasilyev, Tarek Ali El Moselhy, Carlos Pinto Coelho, Laura Proctor and Homer Reid.

Last but not the least, I would like to give my sincere appreciation to my lovely wife Yan and parents, for their love and supports.

Contents

List of Figures

List of Tables

Chapter 1

Introduction

Simulation methods for nanophotonics devices have been studied for decades. Analytical solutions of Maxwell's equations have been favored by many researchers, since they provide direct and accurate insights for designers. For example, eigen-decomposition of the Maxwell's equations are usually employed to analyze nanophotonics. In [16], a dispersion diagram is generated from the eigen-problem, and then used to guide the design of a slow light waveguide in [27]. Perturbation theory [31] is used to analyze slightly modified structures. However, the solution of an eigen-problem is not easily obtained for complicated structures. Instead, it is necessary develop numerical methods to analyze interesting photonics problems.

1.1 Full-Wave Analysis Methods

A very popular full-wave analysis tool is based on the finite-difference-time-domain (FDTD) method [36, 39]. The FDTD method uses the finite difference to approximate derivatives in Maxwell's equations. In most cases, the space is discretized on the basis of the Yee grid [42], having electric and magnetic field components offset for a half grid. Then the method iterates over the time and space domain. The FDTD algorithm requires an absorbing layer to avoid waves reflected back to the computational domain of interest. The perfect matched layer (PML) is the most widely used absorbing layer. The PML was first proposed by Berenger in [3] with split Maxwell's equations, developed in [11, 30, 40] with

an anisotropic medium, and interpreted by a stretched coordinate system in [8]. The FDTD method can provide insight into how fields propagate in time and space. Another advantage of the FDTD method is that a frequency spectrum response can be approximated by computing the response to a single pulse excitation. However, the FDTD method uses a discretization of the entire space domain, so the method is computationally expensive, especially for 3-D simulations.

The integral equation method is another frequently used full-wave method. Both volume integral equation (VIE) [32] and surface integral equation (SIE) methods [14, 29, 33, 37, 38] have been developed for photonics. For inhomogeneous media, volume integration methods (VIE) discretizes the entire volume and and offer few advantages over the FDTD method. For homogeneous or piecewise homogeneous media, a more efficient method is to use a surface integral equation and discretize only surfaces, generating fewer unknowns.

There has been much work on SIE methods. Microstrip antennas are analyzed in [28, 41, 46] based on the mixed potential integration equation (MPIE), which yields a weaker singularity in its integrands than a single potential formulation. To characterize the scattering and radiation properties of arbitrarily shaped microstrip patch antennas in [18], triangular RWG basis functions, which offer great flexibility in the use of non-uniform discretization of the unknown currents on antennas, are employed in SIE formulations. Scattering of 3-D penetrable dielectric bodies have been analyzed in [14, 20, 33] based on a variety of SIE formulations.

To make the SIE method more efficient for complicated geometries, a number of acceleration techniques have been developed, all of which combine iterative matrix solution technique with some form of matrix sparsification. The accelerated techniques include the adaptive integral method (AIM) [4], fast multipole method (FMM) [9,34], the Precorrected-FFT algorithm [21–25, 43–45] and etc.

1.2 Outline of the Thesis

Even with an efficient SIE solver, there is still a problem in accurately simulating some nanophotonic devices due to wave reflections from the ends of structures. In this thesis, we

present a volume conductive absorber technique to eliminate the reflections in the surface integral equation method, so that the physical structure can be correctly modeled and we can obtain accurate insights of the field distribution in the optical components.

In Chapter 2, most of frequently used surface integral equation formulations, including EFIE, MFIE, PMCHW and CFIE are derived and the boundary element method for computing solutions is introduced. In Chapter 3, an example of analyzing an optical waveguide with the PMCHW formulation is given along with an acceleration technique developed for periodic structures. In Chapter 4, we present a volume conductive absorber technique to eliminate the reflections from structure ends. Chapter 5 provides a concise conclusion for this thesis and points out the potential direction in this research topic.

Chapter 2

The Surface Integral Equation Method

In this chapter, we summarize various surface integral formulations formulations derived from Maxwell's equations. We first derive the vector wave equations directly from Maxwell's equations, even though the vector wave equations are hard to solve directly. For this reason, the vector wave equation is often decomposed into independent scalar equations. In 2-D problems, Maxwell's equations can be decomposed into transverse electric (TE) and transverse magnetic (TM) problems, which can be easily solved [10]. For 3-D problems, the wave equations can be decomposed into scalar Helmholtz equations only in sourceless and isotropic homogenous media. For problems excited with sources, vector and scalar potentials, and their corresponding Green's functions are introduced to solve the wave equations. In this thesis, the homogeneous Green's function is used for piecewise homogeneous geometries. The Equivalence Principle is introduced and applied to derive surface integral equation (SIE) formulations for different problems. Finally, the boundary element method (BEM) is employed to solve the SIE models.

2.1 The Wave Equations

2.1.1 The Maxwell Equations

Maxwell's equations are the fundamental equations of electromagnetics. The equations include the Faraday's law, Ampere's law, Gauss's law and a current conservation law. The

differential form of Maxwell's equations are listed below

$$\nabla \times \mathbf{E} = -j\omega\mathbf{B} - \mathbf{M} \tag{2.1}$$

$$\nabla \times \mathbf{H} = j\omega\mathbf{D} + \mathbf{J} \tag{2.2}$$

$$\nabla \cdot \mathbf{D} = \rho_e \tag{2.3}$$

$$\nabla \cdot \mathbf{B} = \rho_m \tag{2.4}$$

$$\nabla \cdot \mathbf{J} = -j\omega\rho_e \tag{2.5}$$

$$\nabla \cdot \mathbf{M} = -j\omega\rho_m \tag{2.6}$$

where **E** is electric field, **H** is magnetic field, **D** is electric flux, **B** is magnetic flux, **J** is electric current density, **M** is magnetic current density, ρ_e is electric charge density, and ρ_m is magnetic charge density. This is a complete set of Maxwell's equations in frequency domain, and the time harmonic term $e^{j\omega t}$ is assumed and depressed [15].

It should be noticed that only four of the six equations are independent. (2.5) and (2.6) can be derived from the first four. Therefore, we can only use the two curl equations (2.1) and (2.2), and two divergence equations, either (2.3), (2.4) or (2.5), (2.6), to describe a given electromagnetic problem. Constitutive relations relate the fluxes and fields as

$$\mathbf{D} = \varepsilon\mathbf{E}, \tag{2.7}$$

$$\mathbf{B} = \mu\mathbf{H}, \tag{2.8}$$

where ε is permittivity and μ is permeability.

2.1.2 Solutions to 2-D Problems

Maxwell's equations correctly describes field and wave phenomenon in time, frequency and space. But solving them directly is difficult as the electric and magnetic fields are coupled. However, for 2-dimensional problems, Maxwell's equations in an isotropic medium can be decoupled into TE and TM problems and analytically solved for simple structures as in [10]. If a geometry is infinitely long in one direction, or fields are invariant in one

direction, then the problem can be considered to be 2-dimensional. Here we assume fields are invariant in z direction, so that we have $\partial/\partial z = 0$, and the medium is homogeneous. Then, the two curl equations (2.1) and (2.2) become two decoupled sets of scalar equations. The TM mode consists of H_x, H_y and E_z components, and the equations are

$$H_x = -\frac{1}{j\omega\mu}\left(\frac{\partial E_z}{\partial y} + M_x\right) \tag{2.9}$$

$$H_y = \frac{1}{j\omega\mu}\left(\frac{\partial E_z}{\partial x} - M_y\right) \tag{2.10}$$

$$E_z = \frac{1}{j\omega\varepsilon}\left(\frac{\partial H_y}{\partial x} - \frac{\partial H_x}{\partial y} - J_z\right), \tag{2.11}$$

where M_x, M_y and J_z are the x, y and z directed magnetic and electric currents, respectively. Substituting (2.9) and (2.10) into (2.11) yields the 2D scalar Helmholtz equation for a TM mode, as

$$\nabla^2_{x,y} E_z + k^2 E_z = j\omega\mu J_z + \frac{\partial M_y}{\partial x} - \frac{\partial M_x}{\partial y} \tag{2.12}$$

where $k = \omega\sqrt{\mu\varepsilon}$ is wave number. The TE mode consists of E_x, E_y and H_z components, and the equations are

$$E_x = \frac{1}{j\omega\varepsilon}\left(\frac{\partial H_z}{\partial y} - J_x\right) \tag{2.13}$$

$$E_y = -\frac{1}{j\omega\varepsilon}\left(\frac{\partial H_z}{\partial x} + J_y\right) \tag{2.14}$$

$$H_z = \frac{1}{j\omega\mu}\left(\frac{\partial E_x}{\partial y} - \frac{\partial E_y}{\partial x} - M_z\right) \tag{2.15}$$

Similarly, substituting (2.13) and (2.14) into (2.1.2) yields the 2D scalar Helmholtz equation for a TE mode, as

$$\nabla^2_{x,y} H_z + k^2 H_z = j\omega\varepsilon M_z + \frac{\partial J_x}{\partial y} - \frac{\partial J_y}{\partial x}. \tag{2.16}$$

Equations (2.12) and (2.16) can be analytically solved given boundary conditions and assuming the geometry is simple.

2.1.3 Solutions to 3-D Problems

For 3D problems, there are usually two ways to solve Maxwell's equations, direct field Helmholtz equations and potential Helmholtz equations. The former can only be obtained in sourceless homogeneous medium, the latter one can be applied to piecewise homogeneous problems with sources.

The Direct Field Equations

Applying the curl operation to (2.1) and (2.2), yields the vector wave equations

$$\nabla \times \nabla \times \mathbf{E} - k^2 \mathbf{E} = -j\omega\mu\mathbf{J} - \nabla \times \mathbf{M} \tag{2.17}$$

$$\nabla \times \nabla \times \mathbf{H} - k^2 \mathbf{H} = -j\omega\varepsilon\mathbf{M} + \nabla \times \mathbf{J}. \tag{2.18}$$

In order to decompose (2.17) and (2.18) to scalar equations, it is necessary to assume there is no source. Then the identity $\nabla \times \nabla \times \mathbf{x} = \nabla(\nabla \cdot \mathbf{x}) - \nabla^2\mathbf{x}$, and the divergence equations (2.3) and (2.4) and be used to derive the Helmholtz equations from (2.17) and (2.18) as

$$\nabla^2 \mathbf{E} + k^2 \mathbf{E} = 0 \tag{2.19}$$

$$\nabla^2 \mathbf{H} + k^2 \mathbf{H} = 0. \tag{2.20}$$

where the three components of electric and magnetic fields are decoupled, resulting in six scalar Helmholtz equations. Then the equations can be analytically solved with proper decoupled boundary conditions for some simple geometries. Equations (2.19) and (2.20) can be interpreted as eigen-decomposition of electromagnetic problems in certain geometries. For problems with excitations, such decoupled equations are not so easily derived.

The Potential Equations

Electromagnetic problems are usually excited by current sources. To solve the wave equations (2.17) and (2.18) with excitations, vector and scalar potentials are introduced to decompose the vector wave equations.

Using the linearity property of Maxwell's equations, it is possible to compute separately

the fields due to electric current and charge $\mathbf{J}$, ρ_e and magnetic current and charge $\mathbf{M}$, ρ_m, and then sum the two fields. First consider the case with electric sources, and $\mathbf{M} = 0$ and $\rho_m = 0$. Then $\nabla \cdot \mathbf{B} = 0$. From the vector derivative identity

$$\mathbf{H} = \frac{1}{\mu} \nabla \times \mathbf{A} \tag{2.21}$$

where $\mathbf{A}$ is referred to as the vector potential. Substituting (2.21) into (2.1) without the $\mathbf{M}$ term results in

$$\nabla \times (\mathbf{E} + j\omega\mathbf{A}) = 0. \tag{2.22}$$

Again, from the vector derivative identity, there is a scalar potential ϕ_e, satisfying $-\nabla\phi_e = \mathbf{E} + j\omega\mathbf{A}$. The field $\mathbf{E}$ can be represented as

$$\mathbf{E} = -j\omega\mathbf{A} - \nabla\phi_e. \tag{2.23}$$

Combining (2.21), (2.23) and (2.2), and then applying the Lorentz condition $\nabla \cdot \mathbf{A} = -j\omega\varepsilon\mu\phi_e$, which removes a degree of freedom in the above potential definition, leads to a Helmholtz equation

$$\nabla^2\mathbf{A} + k^2\mathbf{A} = -\mu\mathbf{J}. \tag{2.24}$$

The above vector Helmholtz equation can be decomposed into three scalar Helmholtz equations. Similarly, combining (2.21), (2.23) and (2.3) yields a scalar Helmholtz equation in terms of ϕ_e as

$$\nabla^2\phi_e + k^2\phi_e = -\frac{\rho_e}{\varepsilon}. \tag{2.25}$$

Note that (2.24) and (2.25) are a set of four scalar Helmholtz equations in four potentials, and can be solved for $\mathbf{J}$ and ρ_e.

Similarly, to solve for fields due to magnetic sources, consider a vector potential $\mathbf{F}$ and a scalar potential ϕ_m, from which the fields can be derived as in

$$\mathbf{E} = \frac{1}{\varepsilon} \nabla \times \mathbf{F}, \tag{2.26}$$

$$\mathbf{H} = -j\omega\mathbf{F} - \nabla\phi_m. \tag{2.27}$$

Then, two Helmholtz equations are obtained,

$$\nabla^2\mathbf{F}+k^2\mathbf{F} = -\varepsilon\mathbf{M}, \tag{2.28}$$

$$\nabla^2\phi_m+k^2\phi_m = -\frac{\rho_m}{\mu}, \tag{2.29}$$

where (2.28) can be decoupled to three scalar Helmholtz equations.

Equations (2.24), (2.25), (2.28) and (2.29) are a set of eight scalar Helmholtz equations for eight scalar components of potentials $\mathbf{A}$, $\mathbf{F}$, ϕ_e and ϕ_m. To generate integral forms of these equations, a Green's function is needed. The Green's function in a spherical coordinate [1] for a scalar Helmholtz equation of the form

$$\nabla^2\Phi+k^2\Phi = -\rho(\mathbf{r}') \tag{2.30}$$

is

$$G(\mathbf{r},\mathbf{r}') = \frac{e^{-jkR}}{4\pi R}, \tag{2.31}$$

where $R = |\mathbf{r}-\mathbf{r}'|$. It should be noted that this is the Green's function for a homogeneous medium and with a radiation boundary condition. The solution to (2.30) can be written in terms of the Green's functions as

$$\Phi(\mathbf{r}) = \int_V G(\mathbf{r},\mathbf{r}')\rho(\mathbf{r}')dV' \tag{2.32}$$

Using the Green's functions, the potentials in (2.24), (2.25), (2.28) and (2.29) can be written as integrals of given current and charge densities as

$$\mathbf{A}(\mathbf{r}) = \mu\int_V G(\mathbf{r},\mathbf{r}')\mathbf{J}(\mathbf{r}')dV' \tag{2.33}$$

$$\mathbf{F}(\mathbf{r}) = \varepsilon\int_V G(\mathbf{r},\mathbf{r}')\mathbf{M}(\mathbf{r}')dV' \tag{2.34}$$

$$\phi_e(\mathbf{r}) = \frac{1}{\varepsilon}\int_V G(\mathbf{r},\mathbf{r}')\rho_e(\mathbf{r}')dV' \tag{2.35}$$

$$\phi_m(\mathbf{r}) = \frac{1}{\mu}\int_V G(\mathbf{r},\mathbf{r}')\rho_m(\mathbf{r}')dV' \tag{2.36}$$

Substituting the potentials into (2.21), (2.23), (2.26) and (2.27), the electric and magnetic

fields due to electric and magnetic currents can be obtained.

2.2 The Equivalence Principle

The Equivalence Principle, also called Huygens' Principle, together with the Uniqueness Theorem, is the basis of several integral formulations of Maxwell's equations. Statements and mathematical formulations of the Uniqueness Theorem and the Equivalence Principle can be found in [7, 12, 17]. Briefly, fields inside a given region can be produced by different source distributions outside the region, and the fields are uniquely determined if the source inside the given region and the tangential components of electric or magnetic fields over the boundary of the given region are specified. An example is illustrated here to show the application of the Equivalence Principle.

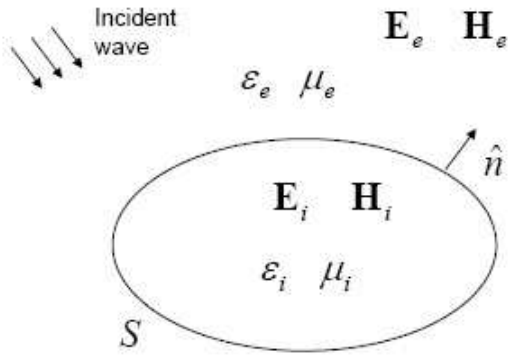

Figure 2-1: Scattering of a dielectric body.

A scattering problem is shown in Fig. 2-1. A homogeneous dielectric body of arbitrary shape and permittivity ε_i and permeability μ_i is embedded in the homogeneous medium of ε_e, μ_e. A plane wave illuminates the system. The fields inside the dielectric body are denoted as $\mathbf{E}_i$, $\mathbf{H}_i$, and the fields outside are denoted as $\mathbf{E}_e$, $\mathbf{H}_e$. $\hat{n}$ is the normal unit vector, pointing outwards. The problem is to compute the field distributions outside of the body. Below are three approaches equivalently modeling the problem. In Approach I, surface electric and magnetic currents are put on the dielectric body surface, and the dielectric body is removed, so that a homogeneous medium with source currents is obtained. Then

the homogeneous Green's function can be applied. Approach Ⅱ and Ⅲ offer alternative ways to replace the dielectric body with a perfect electric conductor (PEC) body and a perfect magnetic conductor (PMC) body, respectively.

Approach I

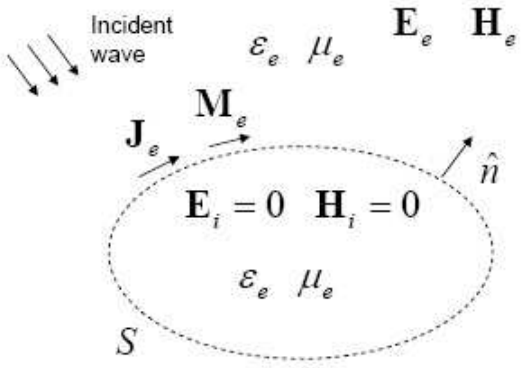

Figure 2-2: Equivalent approach I.

This approach is most frequently used in integral equation formulations. We force the fields inside the dielectric body equal to zero, as $\mathbf{E}_i = 0$, $\mathbf{H}_i = 0$, but the fields outside remain the same. At the same time, the medium of the dielectric body is changed to be the same as the outside as ε_e, μ_e. In order to preserve the field tangential components continuity, equivalent electric and magnetic currents $\mathbf{J}_e$ and $\mathbf{M}_e$ is put on the surface to satisfy the boundary condition as

$$\mathbf{J}_e = \hat{n} \times \mathbf{H}_e|_{S_+} \tag{2.37}$$

$$\mathbf{M}_e = -\hat{n} \times \mathbf{E}_e|_{S_+} \tag{2.38}$$

where $\mathbf{E}_e$ and $\mathbf{H}_e$ are the total fields in the outside region, including the incident and scattered fields. S_+ represents the fields are evaluated at the exterior side of the surface. The equivalent problem is shown in Fig. 2-2. As mentioned above, the problem is to compute the fields outside the body. In the equivalent problem, the actual medium boundary has

been removed and replaced by equivalent currents lying on. Then the fields outside are excited in completely homogenous medium of ε_e, μ_e by the incident wave and the equivalent currents over the virtual boundary. Then, the homogeneous Green's function (2.31) can be used when calculating the excited fields outside due to the equivalent currents. According to the Uniqueness theorem, the fields outside are uniquely determined.

Approach Ⅱ

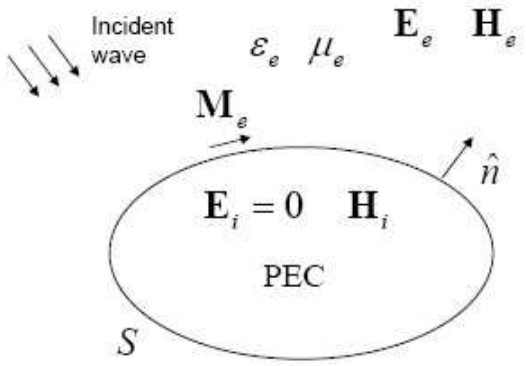

Figure 2-3: Equivalent approach Ⅱ.

In this approach, the dielectric body is replaced by a PEC body, which implies that the electric field is equal to zero as $\mathbf{E}_i = 0$. Similarly, to preserve the tangential components of electric field continuity across the boundary, it is necessary to put magnetic currents on the boundary as

$$\mathbf{M}_e = -\hat{n} \times \mathbf{E}_e|_{S_+} \tag{2.39}$$

where $\mathbf{E}_e$ is the total electric fields in the outside region, including the incident and scattered fields. The PEC body does not affect the continuity of magnetic currents, so we do not need to put equivalent electric currents on the surface. As shown in Fig. 2-3, the equivalent problem becomes a scattering problem of a PEC body in the original medium, excited by an incident plane wave and a sheet of impressed magnetic currents over the PEC surface.

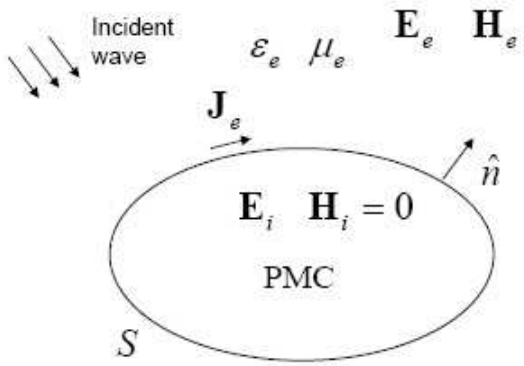

Figure 2-4: Equivalent approach Ⅲ.

Approach Ⅲ

This approach is dual to Approach Ⅱ. Instead of PEC, a PMC body replaces the original dielectric body. Consequently, the magnetic field inside the body becomes zero, then a sheet of electric currents $\mathbf{J}_e$ should be put at the PMC body surface to compensate the jump of the tangential components of magnetic field as

$$\mathbf{J}_e = \hat{n} \times \mathbf{H}_e|_{S_+} \tag{2.40}$$

where $\mathbf{H}_e$ is the total magnetic fields in the outside region, including the incident and scattered fields. Similarly, the continuity of electric fields at the boundary is not broken by the PMC body, so that we do not need to put the artificial magnetic currents. Fig. 2-4 shows the equivalent problem, a scattering problem of a PMC body in the original outside medium, excited by an incident plane wave and a sheet of impressed electric currents over the PMC surface.

So far, we still have not solved the original problem in Fig. 2-1, but presented three different equivalent models for the scattering problem. They are equivalent to the original problem only for the fields in the outside region $\mathbf{E}_e$, $\mathbf{H}_e$. In the next section, we will present formulations to solve the actual problems with derived with the presented Approach I. Actually only Approach I will be used if we insist on using the homogeneous Green's

function. The purpose to present Approach Ⅱ and Ⅲ in this chapter is to show multiple possibilities of the application of Equivalence Principle, and clarify a few confusions people may have, which will be addressed in the next section.

2.3 SIE Formulations

Based on the Uniqueness theorem and the Equivalence Principle, we introduce different surface integral equation formulations, to solve for the field we are interested in.

2.3.1 The EFIE and MFIE Formulations

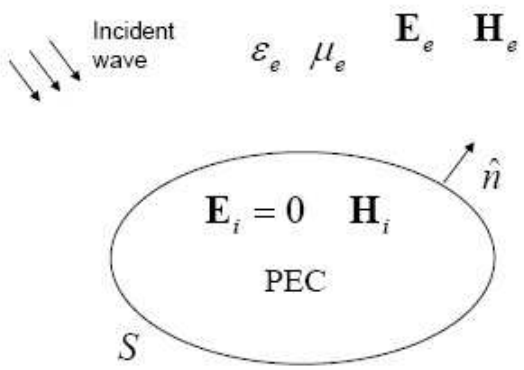

Figure 2-5: Scattering of a PEC body.

Electrical field integral equation (EFIE) and magnetic field integral equation (MFIE) are usually applied to problems consisting of PEC or PMC bodies. Fig. 2-5 shows a scattering problem of a PEC body of arbitrary shape excited by a plane wave, which is actually the problem in Fig. 2-3 without the impressed magnetic currents, for simplicity. In this problem, we are interested in the scattered fields in the outside region. Intuitively, electric currents are induced by the incident wave, and excite the scattered field in the outside region. But to obtain the induced currents quantitatively, we should apply Approach I to get an equivalent model. In the PEC body, we know the electric and magnetic fields are equal to zero. But on the surface of the body, only the electric field is zero, then the magnetic

field has to be forced to be zero as $\mathbf{H}_i = 0$. According to Approach I, to compensate for the discontinuity of the tangential components of magnetic fields across the boundary, a sheet of electric currents is put on the body surface. Then the PEC body can be replaced by the same medium as outside. Now the problem becomes to solve for the outside fields in a homogeneous medium excited by a plane wave and the equivalent electric currents over a virtual surface as in Fig. 2-6. Also, the boundary condition equations (2.37) and (2.38) hold as

$$\hat{n} \times (\mathbf{E}_{inc} + \mathbf{E}_e(\mathbf{J}))|_S = 0 \tag{2.41}$$

$$\hat{n} \times (\mathbf{H}_{inc} + \mathbf{H}_e(\mathbf{J}))|_S = \mathbf{J} \tag{2.42}$$

where the $\mathbf{E}_{inc}$ and $\mathbf{H}_{inc}$ are incident electric and magnetic fields, respectively. $\mathbf{E}_e(\mathbf{J})$ and $\mathbf{H}_e(\mathbf{J})$ are scattered electric and magnetic currents in the outside region due to the equivalent electric currents $\mathbf{J}$, and they can be represented by the mixed potential as in (2.21) and (2.23). Due to the property of a homogeneous medium in the equivalent problem, the homogeneous Green's functions (2.31) for potentials is used to calculate the potentials.

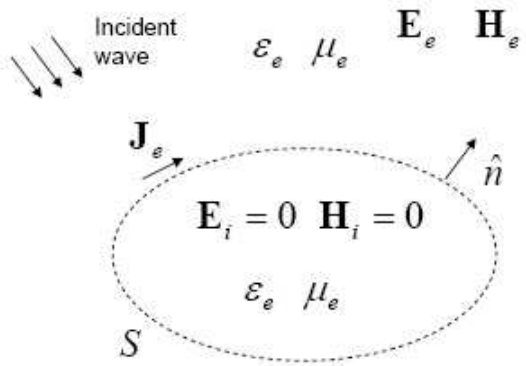

Figure 2-6: Equivalent model of the scattering of a PEC body.

The equation (2.41) is the EFIE, and (2.42) is the MFIE. In the problem of this section, we only have the equivalent electric currents as unknowns, so either EFIE or MFIE could be employed to solve for the unknown currents. The boundary element method will be

introduced to solve the equation numerically in Section 2.4. Once the current $\mathbf{J}$ is obtained, scattered fields anywhere in the outside region can be calculated through (2.21) and (2.23).

Attention should be paid to the difference of the problem here in Fig. 2-5 and the equivalent model in Approach Ⅱ. Fig. 2-5 describes an original scattering problem containing a PCE body to be solved, but Fig. 2-3 is an equivalent model of Fig. 2-1. We can solve the equivalent model in Fig. 2-3 through the model in Fig. 2-6 and EFIE or MFIE presented here, but with an additional sheet of impressed magnetic current. This will implicitly lead to the PMCHW formulation in the next section.

If the PEC body in Fig. 2-5 is replaced by a PMC body, the solution is similar, but to substitute the equivalent electric current by magnetic current, and the magnetic current equal to zero intrinsically.

It is well known that the EFIE or MFIE breaks down at the resonance frequency of the main body. The resonance frequency is defined as the resonant frequency of the body with PEC surface, and filled with the material in the exterior region. The proof can be found in [14].

2.3.2 The PMCHW Formulation

The Poggio-Miller-Chang-Harrington-Wu (PMCHW) [14, 37] formulation is widely used for 3D open structures. It will be derived in this section with the example to solve the scattering problem in Fig. 2-1. Approach I will be applied twice to obtain equivalent models for the exterior fields and interior fields, respectively.

First, applying Approach I leads to an equivalent model for the exterior fields. We force the interior fields equal to zero, replace the interior medium with the exterior medium, and put equivalent electric and magnetic currents $\mathbf{J}_e$ and $\mathbf{M}_e$ on the surface to preserve field continuity as in Fig. 2-7(a). The boundary condition equations (2.37) and (2.38) become

$$-\hat{n} \times (\mathbf{E}_{inc} + \mathbf{E}_e(\mathbf{J}_e, \mathbf{M}_e))|_{S_+} = \mathbf{M}_e \tag{2.43}$$

$$\hat{n} \times (\mathbf{H}_{inc} + \mathbf{H}_e(\mathbf{J}_e, \mathbf{M}_e))|_{S_+} = \mathbf{J}_e \tag{2.44}$$

where S_+ means the fields are evaluated at the interior side of the surface. Then, Approach

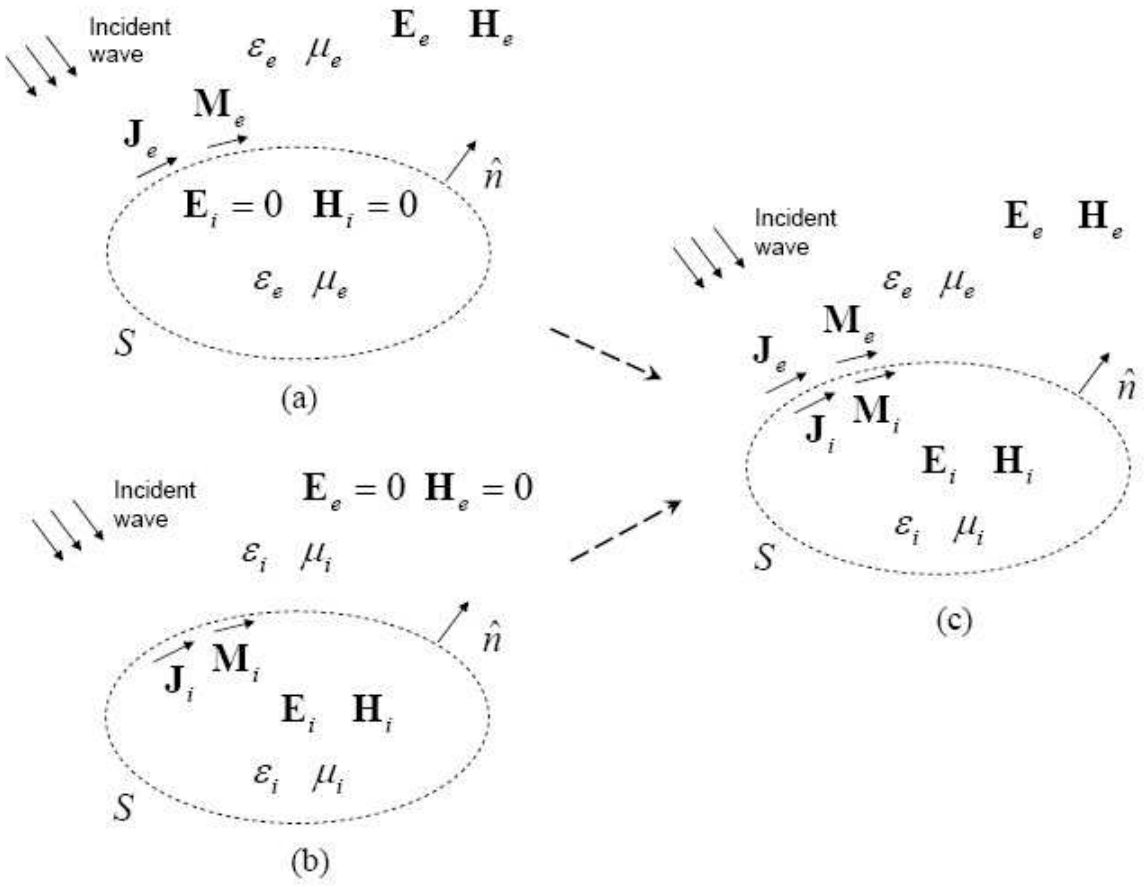

Figure 2-7: Equivalent models of the scattering of a dielectric body. (a) equivalent model for the exterior region; (b) equivalent model for the interior region; (c) combined model for the whole domain

I is applied to get the equivalent model for the interior fields. We force the exterior field to be zero, replace the exterior medium with the interior medium, and put equivalent electric and magnetic currents $\mathbf{J}_i$ and $\mathbf{M}_i$ on the surface to compensate the field jump across the boundary as in Fig. 2-7(b). Similarly, the boundary conditions is

$$\hat{n} \times \mathbf{E}_i(\mathbf{J}_i, \mathbf{M}_i)|_{S_-} = \mathbf{M}_i \tag{2.45}$$

$$-\hat{n} \times \mathbf{H}_i(\mathbf{J}_i, \mathbf{M}_i)|_{S_-} = \mathbf{J}_i \tag{2.46}$$

where S_- represents the fields are evaluated at the interior side of the surface. The first model in Fig. 2-7(a) preserves the exterior fields in the original problem, and the second model in Fig. 2-7(b) preserves the interior fields. Therefore, we can extract the exterior part from Fig. 2-7(a) and the interior part from Fig. 2-7(b) to construct a new model as in Fig. 2-7(c). We know in the original problem, the tangential components of electric and magnetic fields are continuous, thus, we have the field continuity equation as

$$\hat{n} \times (\mathbf{E}_{inc} + \mathbf{E}_e(\mathbf{J}_e, \mathbf{M}_e))|_{S_+} = \hat{n} \times \mathbf{E}_i(\mathbf{J}_i, \mathbf{M}_i)|_{S_-} \tag{2.47}$$

$$\hat{n} \times (\mathbf{H}_{inc} + \mathbf{H}_e(\mathbf{J}_e, \mathbf{M}_e))|_{S_+} = \hat{n} \times \mathbf{H}_i(\mathbf{J}_i, \mathbf{M}_i)|_{S_-} \tag{2.48}$$

Equations (2.47) and (2.48) are PMCHW formulations. Substitute (2.43), (2.44), (2.45), (2.46) into (2.47) and (2.48), the four unknown currents can be reduced to two, as

$$\mathbf{J}_e = -\mathbf{J}_i = \mathbf{J} \tag{2.49}$$

$$\mathbf{M}_e = -\mathbf{M}_i = \mathbf{M} \tag{2.50}$$

As a result, we have two unknown currents $\mathbf{J}$ and $\mathbf{M}$ and correspondingly two equations (2.47) and (2.48).

2.3.3 The CFIE Formulation

The combined field integral equation (CFIE) formulation is similar but more general than PMCHW. We play the same trick as in the last section to obtain two equivalent models for

exterior fields and interior fields as in Fig. 2-7(a) and (b), respectively.

However, in the first model, we evaluate the fields on the interior surface S_-, and in the second model, we evaluate the fields on the exterior surface S_+, and they should be all zeros, as

$$\hat{n} \times (\mathbf{E}_{inc} + \mathbf{E}_i(\mathbf{J}_e, \mathbf{M}_e))|_{S_-} = 0 \tag{2.51}$$

$$\hat{n} \times (\mathbf{H}_{inc} + \mathbf{H}_i(\mathbf{J}_e, \mathbf{M}_e))|_{S_-} = 0 \tag{2.52}$$

$$\hat{n} \times \mathbf{E}_e(\mathbf{J}_i, \mathbf{M}_i)|_{S_+} = 0 \tag{2.53}$$

$$\hat{n} \times \mathbf{H}_e(\mathbf{J}_i, \mathbf{M}_i)|_{S_+} = 0 \tag{2.54}$$

From (2.49) and (2.50) in the last section, we can reduce the four unknown currents to $\mathbf{J}$ and $\mathbf{M}$. As a result, we have four independent equations and two unknown currents. Then we can reduce the four equations to two in various ways. One common option is to combine the electrical field equations and magnetic field equations, respectively, as

$$\hat{n} \times (\mathbf{E}_{inc} + \mathbf{E}_i(\mathbf{J}_e, \mathbf{M}_e))|_{S_-} = \hat{n} \times \mathbf{E}_e(\mathbf{J}_i, \mathbf{M}_i)|_{S_+} \tag{2.55}$$

$$\hat{n} \times (\mathbf{H}_{inc} + \mathbf{H}_i(\mathbf{J}_e, \mathbf{M}_e))|_{S_-} = \hat{n} \times \mathbf{H}_e(\mathbf{J}_i, \mathbf{M}_i)|_{S_+} \tag{2.56}$$

This set equations differs with (2.47) and (2.48) at the field evaluation places. In some published papers, (2.55) and (2.56) are also referred to as PMCHW formulations, since they are proved to be the same in [14].

To combine and weight the electric and magnetic fields at the same evaluation side is another common combining strategy of the four equations (2.51-2.54), as

$$\hat{n} \times [\alpha(\mathbf{E}_{inc} + \mathbf{E}_i(\mathbf{J}_e, \mathbf{M}_e)) + (1-\alpha)(\mathbf{H}_{inc} + \mathbf{H}_i(\mathbf{J}_e, \mathbf{M}_e))]|_{S_-} = 0 \tag{2.57}$$

$$\hat{n} \times [\alpha\mathbf{E}_e(\mathbf{J}_i, \mathbf{M}_i) + (1-\alpha)\mathbf{H}_e(\mathbf{J}_i, \mathbf{M}_i)]|_{S_+} = 0 \tag{2.58}$$

where $\alpha \in (0,1)$ is the weight. An advantage of PMCHW and CFIE is that they do not have the resonant problem, which EFIE and MFIE intrinsically have.

2.4 The Boundary Element Method

It is very hard to analytically solve the formulations introduced in the last section. Thus, numerous numerical methods are developed to approximate the solution within certain accuracy. In this thesis, the boundary element method [13] is employed to discretize surface integral equations, and solve them at reasonable costs.

In this section, we illustrate solving the PMCHW formulation (2.47) and (2.48) with the Galerkin method. Galerkin is a well known boundary element method with the same basis and testing function.

After substitute the current relations (2.49) and (2.50) into (2.47) and (2.48), we only have two unknown currents $\mathbf{J}$ and $\mathbf{M}$, and the equations become

$$-\hat{n}\times(\mathbf{E}_i(\mathbf{J},\mathbf{M})+\mathbf{E}_e(\mathbf{J},\mathbf{M}))|_S = \hat{n}\times\mathbf{E}_{inc}|_S \tag{2.59}$$

$$-\hat{n}\times(\mathbf{H}_i(\mathbf{J},\mathbf{M})+\mathbf{H}_e(\mathbf{J},\mathbf{M}))|_S = \hat{n}\times\mathbf{H}_{inc}|_S. \tag{2.60}$$

To discretize the integral equations, we use a classic basis function – RWG basis function [29]. Fig. 2-8 shows the RWG basis, a pair of triangular panels T_n^+ and T_n^-, which are associated to the nth edge, whose length is l_n. The origin of the global coordinate is o, but the RWG function is represented in a local coordinate in terms of the vectors ρ_n^+ and ρ_n^-, as

$$\mathbf{f}_n(\mathbf{r}) = \begin{cases} \frac{l_n}{2A_n^+}\rho_n^+, & \mathbf{r} \text{ in } T_n^+ \\ \frac{l_n}{2A_n^-}\rho_n^-, & \mathbf{r} \text{ in } T_n^- \\ 0, & \text{else} \end{cases} \tag{2.61}$$

where A_n is area of the corresponding triangle. The RWG basis function automatically enforces the current conservation law, and has a lot of advantages listed in [29]. Then, the unknown currents $\mathbf{J}$ and $\mathbf{M}$ can be discretized in terms of the RWG basis function as

$$\mathbf{J}(\mathbf{r}') = \sum_n J_n\mathbf{f}_{Jn}(\mathbf{r}') \tag{2.62}$$

$$\mathbf{M}(\mathbf{r}') = \sum_n M_n\mathbf{f}_{Mn}(\mathbf{r}') \tag{2.63}$$

where J_n and M_n are the coefficients of the expansions to be determined. After plugging

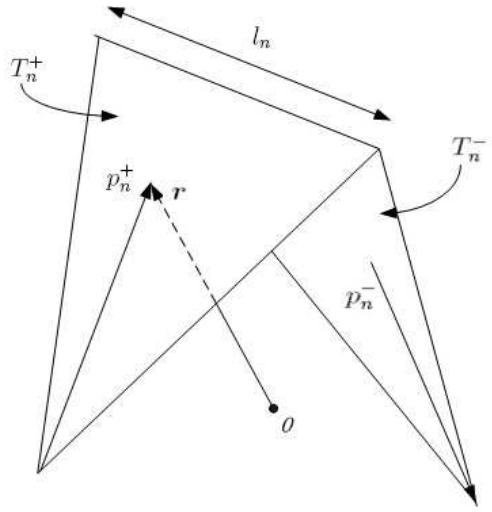

Figure 2-8: The RWG basis function

(2.62) and (2.63) into (2.59) and (2.60), we are now solving for the coefficients J_n and M_n. According to the formulations in Section 2.1.3, we can represent the electric and magnetic fields in terms of operators L and K as

$$\mathbf{E}_l(\mathbf{J},\mathbf{M}) = -Z_l L_l(\mathbf{J}) + K_l(\mathbf{M}) \tag{2.64}$$

$$\mathbf{H}_l(\mathbf{J},\mathbf{M}) = -K_l(\mathbf{J}) - \frac{1}{Z_l} L_l(\mathbf{M}) \tag{2.65}$$

where $Z_l = \sqrt{\mu_l/\varepsilon_l}$. $l = e$ or i represents the region where the fields are evaluated. The operators are defined as

$$L_l(\mathbf{X}) = jk_l \int_S \left[\mathbf{X}(\mathbf{r}') + \frac{1}{k_l^2}\nabla\nabla'\cdot\mathbf{X}(\mathbf{r}')\right] G_l(\mathbf{r},\mathbf{r}')dS' \tag{2.66}$$

$$K_l(\mathbf{X}) = -\int_S \nabla \times G_l(\mathbf{r},\mathbf{r}')\mathbf{X}(\mathbf{r}')dS' \tag{2.67}$$

where $k_l = \omega\sqrt{\varepsilon_l\mu_l}$ is the wave number in region l. $X(\mathbf{r}')$ is the basis function for electric or magnetic currents. $G_l(\mathbf{r},\mathbf{r}')$ is the Green's function in homogeneous medium l as (2.31).

Assume the surface of the body has been discretized by N RWG functions. Then we need to discretize the integral equations (2.59) and (2.60) with respect to the N RWG functions and test the fields with the same RWG functions. Then we finally discretize the

integral equations and construct a linear system as

$$\begin{bmatrix} \mathbf{A}_{11} & \mathbf{A}_{12} \\ \mathbf{A}_{21} & \mathbf{A}_{22} \end{bmatrix} \begin{bmatrix} J \\ M \end{bmatrix} = \begin{bmatrix} b_E \\ b_H \end{bmatrix} \tag{2.68}$$

where J and M are the unknown coefficients to be solved, and the elements in the sub-matrices are the tested fields as

$$A_{11} = Z_e \int_S \mathbf{g}(\mathbf{r}) \cdot L_e(\mathbf{J}) dS + Z_i \int_S \mathbf{g}(\mathbf{r}) \cdot L_i(\mathbf{J}) dS \tag{2.69}$$

$$A_{12} = -\int_S \mathbf{g}(\mathbf{r}) \cdot K_e(\mathbf{M}) dS - \int_S \mathbf{g}(\mathbf{r}) \cdot K_i(\mathbf{M}) dS \tag{2.70}$$

$$A_{21} = \int_S \mathbf{g}(\mathbf{r}) \cdot K_e(\mathbf{J}) dS + \int_S \mathbf{g}(\mathbf{r}) \cdot K_i(\mathbf{J}) dS \tag{2.71}$$

$$A_{22} = \frac{1}{Z_e} \int_S \mathbf{g}(\mathbf{r}) \cdot L_e(\mathbf{M}) dS + \frac{1}{Z_i} \int_S \mathbf{g}(\mathbf{r}) \cdot L_i(\mathbf{M}) dS \tag{2.72}$$

$$b_E = \int_S \mathbf{g}(\mathbf{r}) \cdot \mathbf{E}_{inc}(\mathbf{r}) dS \tag{2.73}$$

$$b_H = \int_S \mathbf{g}(\mathbf{r}) \cdot \mathbf{H}_{inc}(\mathbf{r}) dS \tag{2.74}$$

where $\mathbf{g}(\mathbf{r})$ is the corresponding testing function.

(2.68) is a dense linear system, and it is usually solved iteratively. In this thesis, we solve it through the GMRES scheme [2].

Chapter 3

Numerical Analysis of An Optical Waveguide

This chapter presents details to analyze an optical dielectric waveguide with the boundary element method, based on the PMCHW formulation. A circulant matrix vector product technique is applied to reduce memory requirements and computational time. Numerical results show the accuracy and efficiency of the presented method.

3.1 Formulations

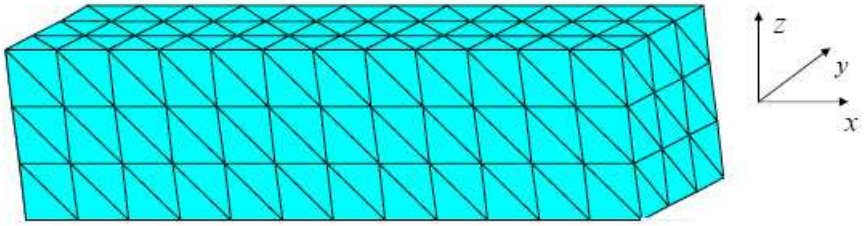

Figure 3-1: A dielectric waveguide.

An optical waveguide is shown in Fig. 3-1. The PMCHW [14, 37] formulation, introduced in the last chapter, is employed to model this waveguide. It is illustrated with a cross section of the waveguide in Fig. 3-2. $\mathbf{J}_e$, $\mathbf{M}_e$ and $\mathbf{J}_i$, $\mathbf{M}_i$ are equivalent currents lying on

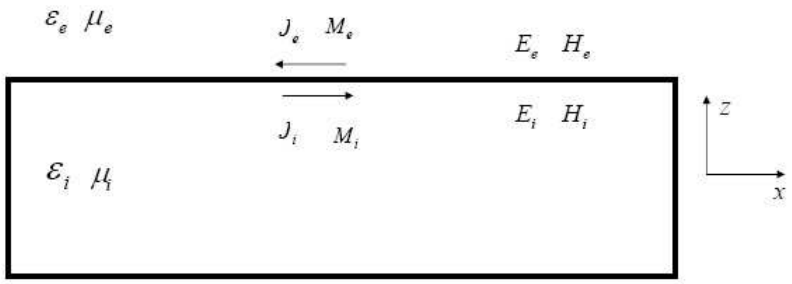

Figure 3-2: The cross section of one waveguide.

the exterior side and interior side of the waveguide surface, respectively. On the waveguide surface, the equations (2.47) and (2.48) are written here, with the tangential electric and magnetic fields continuous as

$$\hat{n} \times [\mathbf{E}_{inc} + \mathbf{E}_e(\mathbf{J}_e, \mathbf{M}_e)] = \hat{n} \times \mathbf{E}_i(\mathbf{J}_i, \mathbf{M}_i) \tag{3.1}$$

$$\hat{n} \times [\mathbf{H}_{inc} + \mathbf{H}_e(\mathbf{J}_e, \mathbf{M}_e)] = \hat{n} \times \mathbf{H}_i(\mathbf{J}_i, \mathbf{M}_i). \tag{3.2}$$

where $\hat{n}$ is the unit vector pointing to the exterior region. $\mathbf{E}_{inc}$ and $\mathbf{H}_{inc}$ are the incident electric and magnetic fields from the left end, respectively. Then the PMCWH is solved by the boundary element method in section 2.4 by constructing and solving the linear system (2.68).

3.2 Acceleration and Preconditioning with FFT

The linear system (2.68) is solved with iterative algorithms, such as GMRES for a non-symmetrically dense system. The dense matrix requires $O(N^2)$ storage, where N is the number of unknowns, which is very expensive for 3D simulations. In the present case, the waveguide is usually long, so that N is very large. The technique in this section will sparsify the $\mathbf{A}$ matrix and accelerate the matrix vector product in each iterative step. Fig. 3-3 shows a periodic unit of the waveguide. The periodicity makes the four sub-matrices of $\mathbf{A}$ block Toeplitz matrices. We denote the sub-matrix of $\mathbf{A}$ is $\mathbf{A}_{ij}$ and $i, j = 1, 2$. A Toeplitz

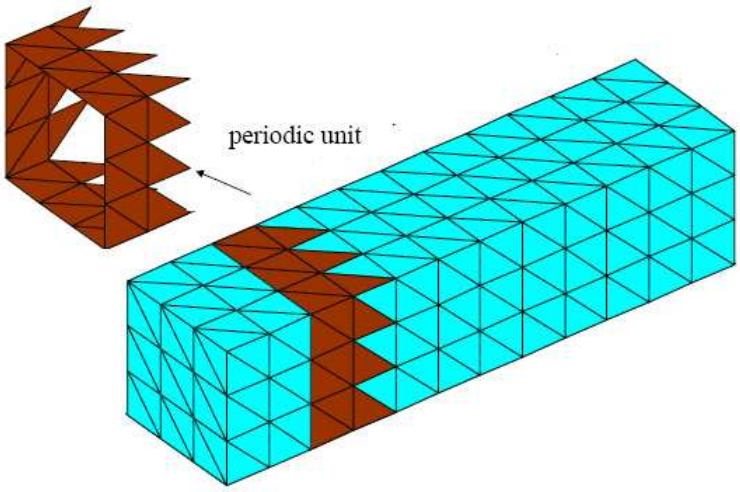

Figure 3-3: Optical Ring resonator filter with absorbers at the ends of transmission lines.

matrix can be implicitly padded into a circulant matrix, and the circulant matrix-vector product is then computed with the FFT [19]. For the present block Toeplitz matrix, it is first transformed into a matrix with Toeplitz blocks by a simple permutation, then compute the matrix-vector product with the above technique, as

$$\mathbf{A}_{ij}\mathbf{x} = IFFT\left\{FFT[Perm(\mathbf{A}_{ij}^{Toep})]\cdot FFT(\mathbf{x}_j)\right\} \tag{3.3}$$

where *Perm* is the permutation operator, and $\mathbf{x}_j$ is a corresponding sub-vector of $\mathbf{x}$. As the result, we only need to store one row and one column of each Toeplitz block denoted as $\mathbf{A}_{ij}^{Toep}$, with only $O(N)$ memory storage. The computation requirement is reduced to $O(N\log N)$, rather than $O(N^2)$.

Another great advantage of working with a Toeplitz or a block Toeplitz matrix is the existence of a highly efficient preconditioner [5, 35]. A circulant matrix is approximated from the Toeplitz matrix, and then easily inverted with the FFT. For the present block Toeplitz matrix, permutations are necessary to construct a corresponding block circulant matrix approximation as in [6]. Then, the preconditioner of $\mathbf{A}_{ij}$ becomes

$$\mathbf{P}_{ij} = FFT[Perm(\mathbf{A}_{ij}^{Toep})]. \tag{3.4}$$

Through observation, the sub-matrices $\mathbf{A}_{11}$ and $\mathbf{A}_{22}$ are block diagonal dominant in the matrix $\mathbf{A}$, so that we only need to generate the block preconditioning matrix for the dominant ones. Then we have the preconditioning matrix as

$$\mathbf{P} = \begin{bmatrix} \mathbf{P}_{11} & 0 \\ 0 & \mathbf{P}_{22} \end{bmatrix}. \tag{3.5}$$

This preconditioner works very well. The GMRES converges within 100 iterations.

3.3 Numerical Results

A dielectric waveguide is experimented with in this section. The length unit in this thesis is wavelength. The area of the cross section of the waveguide is 0.75×0.75. Fig. 3-4 shows electric fields along the x axis at the center of the cross section as the length of waveguide is 4, 8, and 16 respectively. Both real magnitude and complex magnitude are included in each figure. From the complex magnitude, wave patterns clearly show the combination of the traveling and standing waves, which means that waves are reflected back from the ends of the waveguide. This makes sense that the waveguide is of finite length, and the impedance mismatch at the ends makes wave reflected back.

Moreover, it is observed that the complex magnitudes are not exactly the same along the x axis. They are quite strongly perturbed for the short waveguide in Fig. 3-4(a), and show a weak envelope for the long waveguide in Fig. 3-4(c). That is because the waveguide is excited by a uniform sheet of current at the left end, and the source also excites radiation modes, evanescent modes, leaky modes and etc. rather than the pure propagation modes. As a result, the mixed modes disturb the propagation modes for the short waveguide, since it takes a distance to eliminate the evanescent modes. For the long waveguide, the radiation modes and leaky modes form a weak envelope, and it will take an even longer distance to remove its effects.

Meanwhile, the computational costs for the above three cases by the direct BEM and the accelerated BEM as in Section 3.2 are listed in Table 3.1. We ran the simulations in a workstation with an Intel Core2Duo X6800 3GHz CPU, and 2GB memory. It shows the

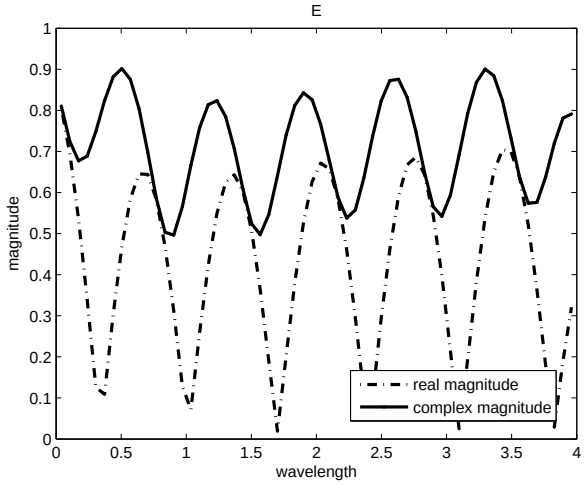

(a) 4 wavelengths

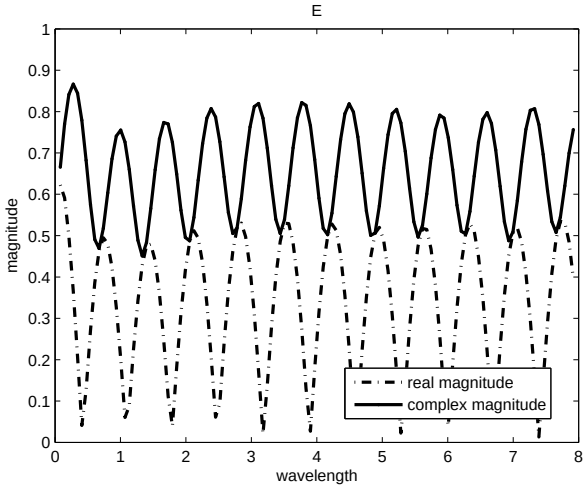

(b) 8 wavelengths

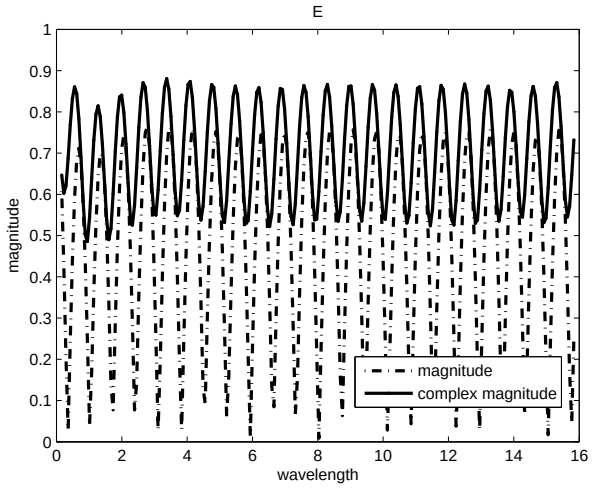

(c) 16 wavelengths

Figure 3-4: The magnitude of the electric field along x axis inside the waveguide.

accelerated BEM is much cheaper than the regular one. The regular BEM even runs out of memory for the 16 wavelengths waveguide. And it is observed that both the time and memory are roughly on the order of $O(N^2)$ for the regular BEM, and roughly $O(NlogN)$ in time, and $O(N)$ in memory, for the accelerated BEM, which is consistent with the analysis in Section 3.2.

Table 3.1: The comparison of the regular BEM and accelerated BEM

Waveguide length (wavelength)	Number of unknown	Regular		Accelerated	
		Time	Memory	Time	Memory
4	2988	679 sec	143 M	188 sec	30 M
8	5868	3028 sec	550 M	378 sec	60 M
16	11628	N.A.	N.A.	757 sec	120 M

A reasonable solver should provide results converging to the right solution as we refine the discretization. Fig. 3-5 shows the converging solutions when the discretization in the cross section is gradually improved. The number in the legend is the number of triangles along one side. It is observed that we still get the qualitatively reasonable wave pattern for coarse discretization, and the solution becomes accurate when the size of each triangle is around $1/10$ wavelength.

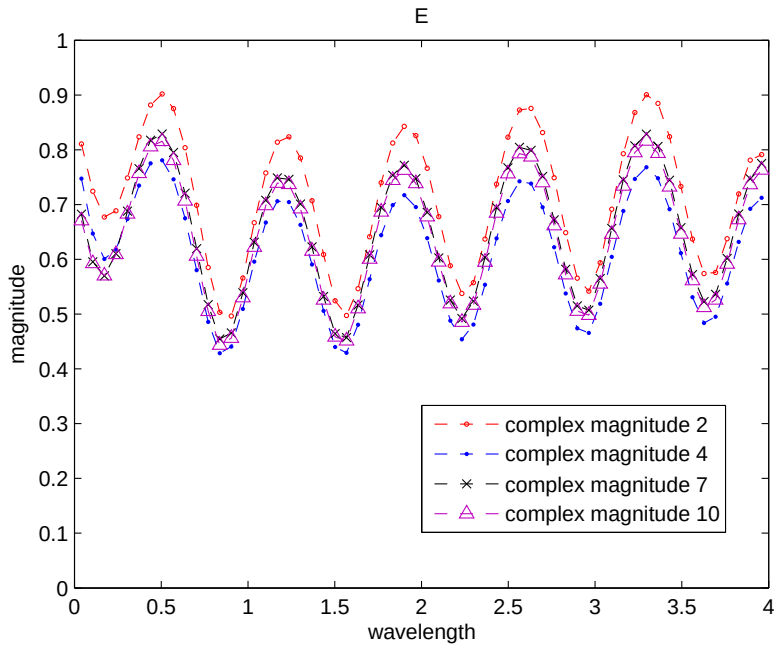

Figure 3-5: Magnitude of electric fields with different discretization.

Chapter 4

Conductive Absorbers

In this chapter, we show the conventional surface integral equation solver may run into problems when simulating some photonics devices, which requires to be extended to infinity to avoid reflections. We present an approach, adding a volume conductive absorber at the end of the device to absorb incoming waves. We stick to the surface integral equation method, since the piecewise homogeneous media is still preserved. The numerical methods show that the present technique can effectively absorb the incoming wave and reduce the reflection waves. However, this approach is not able to reduce reflection to be very small, and the reason is analyzed in this chapter.

4.1 Background

This section shows two examples of nanophotonics devices to be modeled and simulated by an SIE solver. However, to accurately model either device, both devices have surfaces which must extend to infinity.

Fig. 4-1 shows an optical filter with coupled transmission lines and a ring resonator [26]. The filter selects certain frequency waves from the input, and removes the rest. In order to model this filter correctly, it is necessary to make sure that wave propagates as traveling wave in the transmission line, guaranteeing no wave reflected back from the right end to disturb the coupling mechanism. However, we have to extend the transmission line to infinity to generate traveling wave.

Another example in Fig. 4-2 shows a similar problem. A slow light waveguide [27] of an optical delay line system is shown in Fig. 4-2(a). The taper in Fig. 4-2(b) is designed to couple power into the waveguide and minimize reflection loss. A good taper can reduce the field reflection to 1×10^{-3}, or 1×10^{-6} in terms of power. As a result, a 3-D SIE solver used to analyze this structure must not generate numerical reflections or it will be impossible to measure the reflection only due to the taper.

However, the conventional SIE solver cannot eliminate reflections for a structure with finite surface. Fig. 4-2(c) shows a possible solution using a periodic boundary condition to model an infinitely long waveguide so that there won't be any reflection from the end of the structure. However, for a dielectric waveguide, it takes a very long distance for the solution to become periodic due to the inevitably excited evanescent modes, radiation modes, and leaky modes. Moreover, it is hard to analytically obtain the periodicity for complicated guided structures, so that this solution is not easily realizable. Another solution to this infinite extension problem for the SIE solver is to add a very long volume conductive absorber at the end of the waveguide as shown in Fig. 4-2(d). We discuss the formulations of this solution in Section 4.2, and show numerical results in Section 4.3.

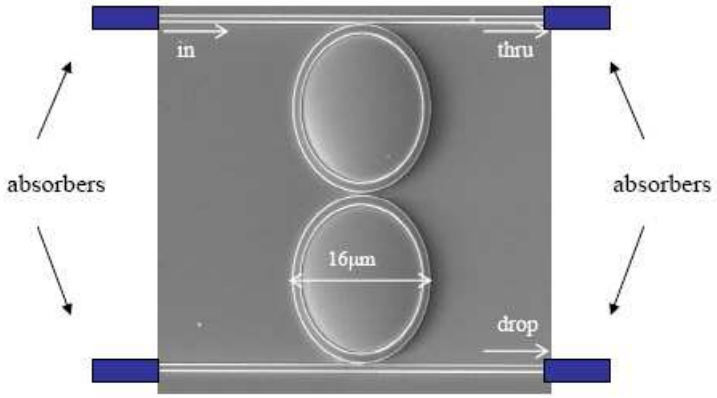

Figure 4-1: Optical Ring resonator filter with absorbers at the ends of transmission lines [26].

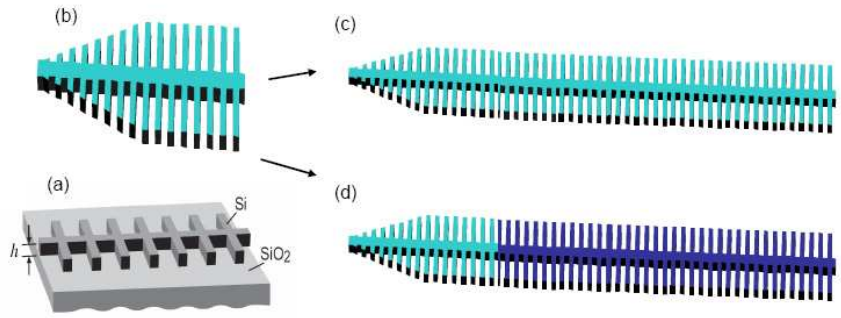

Figure 4-2: Simulation schemes for optical taper. (a) a slow light waveguide [27]; (b) a taper for the slow light waveguide; (c) a taper with a very long slow light waveguide; (d) a taper with a very long volume conductive absorber of small conductance

4.2 Volume Conductive Absorbers

4.2.1 An absorber

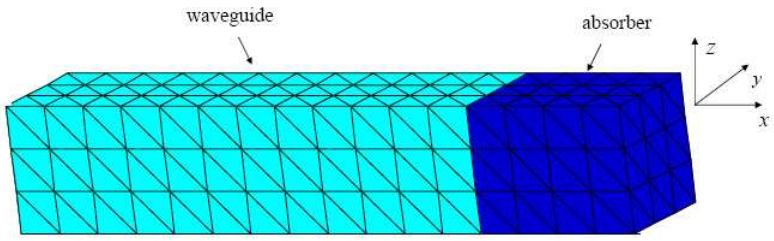

Figure 4-3: Discretized dielectric waveguide with an absorber.

This section presents the approach to add a volume conductive absorber at the end of the transmission line, to eliminate reflections. A long dielectric waveguide with a volume conductive absorber of constant conductance is embedded in a homogeneous medium as shown in Fig.4-3. This system is analyzed by the boundary element method with the PMCHW formulation as introduced in Chapter 2. The surfaces and the interface are discretized with triangles. The whole system is divided into three sub-regions as shown in Fig. 4-4. The Equivalence Principle and Approach I in Chapter 2 are applied to obtain a equivalent model for each sub-region, and construct a PMCHW formulation, to solve for the equiv-

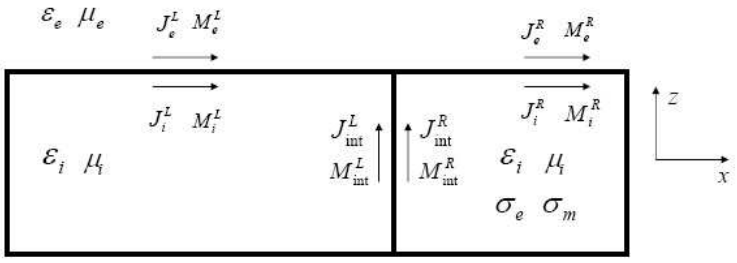

Figure 4-4: The cross section of a waveguide with a volume conductive absorber.

alent currents $\mathbf{J}$ and $\mathbf{M}$ lying on the surface and interface. We divide all the surfaces into three parts S^L, S^R and S^{int}, denoting the surface of the left waveguide, right absorber and the interface, respectively. First, we enforce the PMCHW on S^L

$$\hat{n} \times [\mathbf{E}_{inc} + \mathbf{E}_e^L(\mathbf{J}_e^L, \mathbf{M}_e^L, \mathbf{J}_e^R, \mathbf{M}_e^R)] = \hat{n} \times \mathbf{E}_i^L(\mathbf{J}_i^L, \mathbf{M}_i^L, \mathbf{J}_{int}^L, \mathbf{M}_{int}^L) \tag{4.1}$$

$$\hat{n} \times [\mathbf{H}_{inc} + \mathbf{H}_e^L(\mathbf{J}_e^L, \mathbf{M}_e^L, \mathbf{J}_e^R, \mathbf{M}_e^R)] = \hat{n} \times \mathbf{H}_i^L(\mathbf{J}_i^L, \mathbf{M}_i^L, \mathbf{J}_{int}^L, \mathbf{M}_{int}^L), \tag{4.2}$$

in which the fields are evaluated in the exterior region and the interior region of the left waveguide, respectively. Similarly, we obtain the PMCHW on S^R, as

$$\hat{n} \times [\mathbf{E}_{inc} + \mathbf{E}_e^R(\mathbf{J}_e^L, \mathbf{M}_e^L, \mathbf{J}_e^R, \mathbf{M}_e^R)] = \hat{n} \times \mathbf{E}_i^R(\mathbf{J}_i^R, \mathbf{M}_i^R, \mathbf{J}_{int}^R, \mathbf{M}_{int}^R) \tag{4.3}$$

$$\hat{n} \times [\mathbf{H}_{inc} + \mathbf{H}_e^R(\mathbf{J}_e^L, \mathbf{M}_e^L, \mathbf{J}_e^R, \mathbf{M}_e^R)] = \hat{n} \times \mathbf{H}_i^R(\mathbf{J}_i^R, \mathbf{M}_i^R, \mathbf{J}_{int}^R, \mathbf{M}_{int}^R). \tag{4.4}$$

where fields are evaluated in the exterior region and the interior region of the right absorber, respectively. Finally, the PMCHW on the interface S^{int} is obtained as

$$\hat{n} \times [\mathbf{E}_{int}^L(\mathbf{J}_i^L, \mathbf{M}_i^L, \mathbf{J}_{int}^L, \mathbf{M}_{int}^L)] = \hat{n} \times \mathbf{E}_{int}^R(\mathbf{J}_i^R, \mathbf{M}_i^R, \mathbf{J}_{int}^R, \mathbf{M}_{int}^R) \tag{4.5}$$

$$\hat{n} \times [\mathbf{H}_{int}^L(\mathbf{J}_i^L, \mathbf{M}_i^L, \mathbf{J}_{int}^L, \mathbf{M}_{int}^L)] = \hat{n} \times \mathbf{H}_{int}^R(\mathbf{J}_i^R, \mathbf{M}_i^R, \mathbf{J}_{int}^R, \mathbf{M}_{int}^R). \tag{4.6}$$

where the fields are evaluated in the interior regions of the left waveguide and right absorber, respectively. So far, we have six equations as well as six unknown currents, then

the boundary element method in Section 2.4 is applied to solve for the current distribution.

The conductivity of the absorber makes incoming wave decay exponentially. We set both electric and magnetic conductance σ_e and σ_m for the absorber to satisfy

$$\frac{\sigma_e}{\sigma_m} = \frac{\varepsilon_i}{\mu_i}, \tag{4.7}$$

in order to match the impedance at the interface to avoid the reflections from normal incidence. Since the SIE solver only works for homogeneous isotropic media in each subregion, the conductance should be constant scalar all the way in the absorber.

4.2.2 An Absorber with A Ring

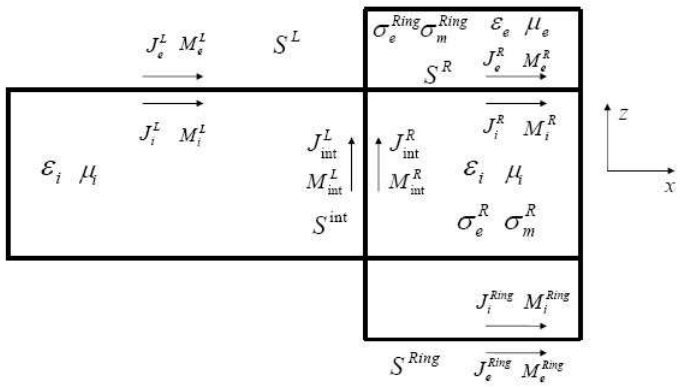

Figure 4-5: The cross section of a waveguide with a volume conductive absorber with a ring.

The absorber in Fig.4-3 can only absorb the incoming waves from the waveguide. But there is propagating waves outside the waveguide. Though the magnitudes of the outside waves exponentially decays along y and z directions, the waves close to the waveguide surface may still have effects on the interior wave through coupling across the boundary. This section presents an absorber with a ring as shown in Fig. 4-5. This absorber can eliminate both the wave coming from the waveguide and the wave outside but close to the waveguide surface.

In Fig. 4-5, unknown currents $\mathbf{J}$ and $\mathbf{M}$ lie on four surfaces S^L, S^R, S^{int} and S^{Ring}.

Therefore, four sets of PMCHW equations are formed on each surface in a similar way as in the last section. But it should be noticed that the conductance for the two absorbers are different and should satisfy

$$\frac{\sigma_e^R}{\sigma_m^R} = \frac{\varepsilon_i}{\mu_i}, \tag{4.8}$$

$$\frac{\sigma_e^{Ring}}{\sigma_m^{Ring}} = \frac{\varepsilon_e}{\mu_e}, \tag{4.9}$$

in order to enforce the impedance matched on each interface, respectively.

4.3 Numerical Results

We simulate a couple of examples to study the effects of the presented approaches. The FFT acceleration technique in Section 3.2 is applied to simulate long absorbers. The dimension unit here is the wavelength inside the waveguide. A dielectric waveguide of 10 wavelengths with a volume conductive absorber of 30 wavelengths is experimented with here. The area of the cross section is 0.75×0.75. The material of the waveguide is silicon of $\varepsilon_i = 13$ and the exterior region is SiO_2 of $\varepsilon_e = 3.7$. Fig. 4-6 shows the complex magnitudes of the electric fields inside the waveguide and absorber with different loss tangent along the x axis. The dashed line shows the position of the interface. It clearly shows that the absorber with big loss (0.1) can completely eliminate incoming wave, but generates quite big numerical reflections. The numerical reflections are reduced when the loss goes down to 0.02. But when the loss is further reduced to 0.005, the absorber cannot kill the wave completely so that large reflections are produced.

Then we experiment a case with very long absorber. A waveguide of 15 wavelengths with an absorber of 55 wavelengths and loss tangent 0.01 is used. Fig. 4-7 shows the complex magnitude of electric field inside the waveguide and the absorber. It is observed that waves are completely eliminated in the absorber. But there are still visible magnitude ripples (numerical reflections) in the waveguide. The standing wave ratio (SWR) and field reflection 1.0196 and 0.0097, respectively, which means there is approximately 1% reflections at the interface.

A waveguide of 3 wavelengths an an absorber with a ring of 2 wavelengths is tested. The loss tangent is 0.2. Fig. 4-8 shows the comparison of magnitudes of electrical field along the x direction inside the waveguide and absorber with and without the ring. It shows that the absorber with a ring does make the wave decay faster in the absorber, but it still has the same order of reflections as the absorber without a ring. Therefore, the ring absorber does not help reduce the reflection.

It is the three problems that may cause the small reflections observed through the above experiments: 1) The restriction of isotropic media for SIE solvers makes it impossible to absorb obliquely incident waves. 2) The volume conductance has to be constant in order to preserve the homogeneous medium in the absorber body. This fact prevents us from smoothly turning on the conductance, and since we are solving a discretized version of Maxwell's equations, this sudden change in conductance generates numerical reflections. 3) The interface of the waveguide and the absorber has to be discretized, whose numerical error may lead to reflection.

With the current SIE formulation, the first problem is hard to solve. But fortunately, we have mostly normally incident waves for transmission lines, so that we reduce the reflection to be quite small. To solve the second problem, we have to make the conductance very small to avoid a large jump of material property at the interface, so that the absorber should be long enough to completely absorb the incoming wave. The third problem is an intrinsic problem of numerical simulations even if the discretization is refined.

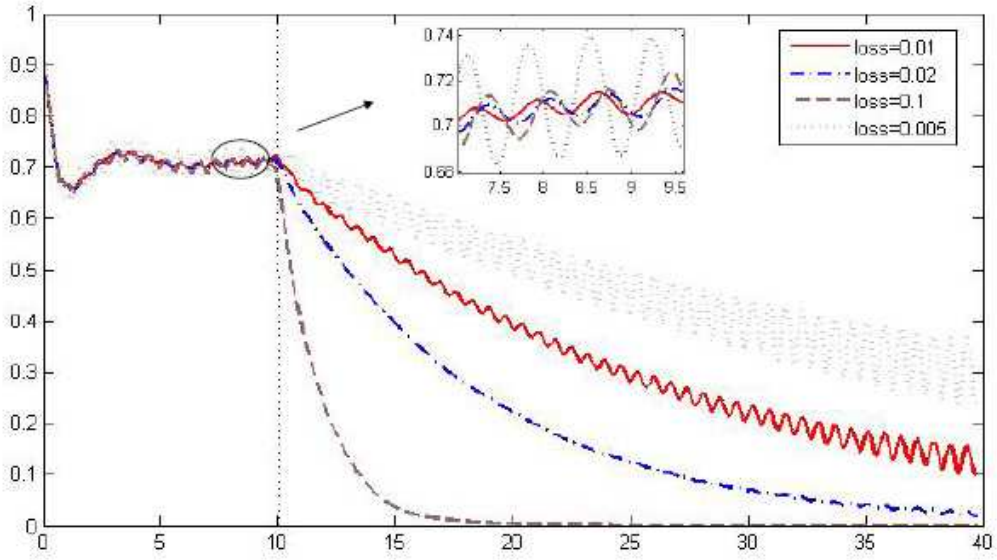

Figure 4-6: The complex magnitude of electrical field along x inside the waveguide and volume conductive absorber with different loss.

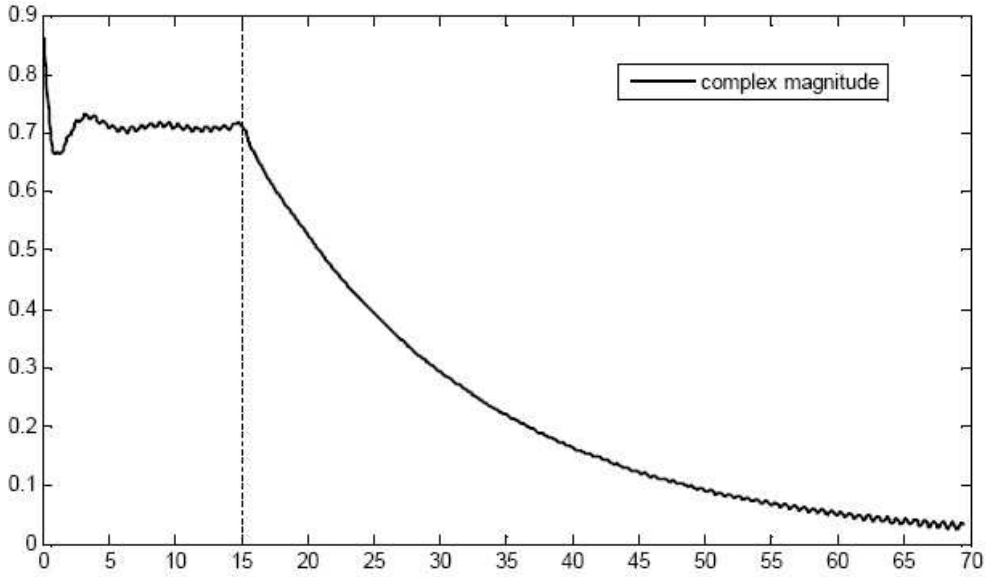

Figure 4-7: The complex magnitude of electrical field along x inside the waveguide with volume conductive absorber.

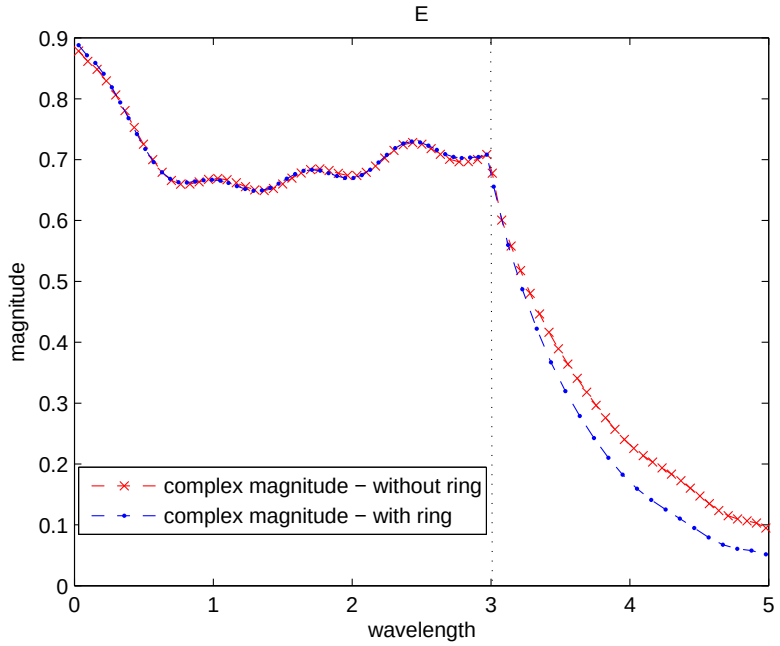

Figure 4-8: The complex magnitude of electrical field along x inside the waveguide and the absorber with and without a ring.

Chapter 5

Conclusions

In this thesis, we introduced methods to solve Maxwell's equations, and derived various surface integral equation formulations including EFIE, MFIE, PMCHW and CFIE, based on the Uniqueness Theorem and the Equivalence Principle. Then we employ the boundary element method to solve those formulations. An optical waveguide was analyzed by the boundary element method based on the PMCHW formulation, and accelerated by the circulant matrix vector product technique due to the periodic property. However, the field pattern inside the waveguide clearly verifies that waves reflect from the ends of waveguide, making the method unusable for characterizing some nanophotonics devices.

Then, we presented a numerical technique to include a volume conductive absorber at the ends of the optical component to eliminate the reflections, so that wave behavior inside the optical device can be observed accurately. A dielectric optical waveguide with the absorber technique was modeled. The numerical results show the volume conductive absorber can reduce the reflection to 1%. To further reduce the reflection, a new technique should be developed to have the following two properties: 1) the interface does not need to be discretized so that no numerical reflection exists; 2) the conductance can be smoothly varied along the waveguide so that is no sudden jump of material property across the interface.

Bibliography

[1] C. A. Balanis. *Advanced Engineering electromagnetics*. John Wiley, 1989.

[2] Richard Barrett, Michael W. Berry, Tony F. Chan, James Demmel, June Donato, Jack Dongarra, Victor Eijkhout, Roldan Pozo, Charles Romine, and Henk van der Vorst. *Templates for the Solution of Linear Systems: Building Blocks for Iterative Methods*. SIAM, 1987.

[3] J. P. Berenger. A perfectly matched layer for the absorption of electromagnetic waves. *J. Comp. Phy.*, 114:185–200, 1994.

[4] E. Bleszynski, M. Bleszynski, and T. Jaroszewicz. AIM: Adaptive integral method for solving large-scale electromagnetic scattering and radiation problems. *radio Sci.*, 31:1225–1251, 1996.

[5] Tony F. Chan. An optimal circulant preconditioner for Toeplitz systems. *SIAM journal on scientific and statistical computing*, 9(4):766–771, 1988.

[6] Tony F. Chan and Julia A. Olkin. Circulant preconditioners for Toeplitz-block matrices. In *SIAM Conference on Linear Algebra in Signals, Systems, and Control*, pages 89–101, 1990.

[7] Kun-Mu Chen. A mathematical formulation of the Equivalence principle. *IEEE Trans. Microwave Theory Tech.*, 37(10):1576– 1581, 1989.

[8] Weng Cho Chew and William H. Weedon. A 3-D perfectly matched medium from modified Maxwell's equations with stretched coordinates. *Microwave Opt. Technol. Lett.*, 7(13):599– 604, 1994.

[9] R. Coifman, V. Rokhlin, and S. Wandzura. The fast multipole method for the wave equation: A pedestrian prescription. *IEEE Antennas Propag. Mag.*, 35:7–12, 1993.

[10] Donald G. Dudley. *Mathematical Foundations for Electromagnetic Theory*. Wiley-IEEE Press, 2001.

[11] Stephen D. Gedney. An anisotropic perfectly matched layer-absorbing medium for the truncation of FDTD lattices. *IEEE Trans. Antennas Propagat.*, 44(12):1630– 1639, 1996.

[12] Roger F. Harrington. *Time-Harmonic Electromagnetic Fields*. McGraw-Hill Book Company, 1961.

[13] Roger F. Harrington. *Field computation by moment methods*. Macmillan, 1968.

[14] Roger F. Harrington. Boundary integral formulations for homogeneous material bodies. *Journal of Electromagnetic Waves and Applications*, 3(1):1–15, 1989.

[15] John David Jackson. *Classical Electrodynamics*. third edition.

[16] Steven G. Johnson and J. D. Joannopoulos. Block-iterative frequency-domain methods for Maxwell's equations in a planewave basis. *Optics Express*, 8(3):173–190, 2001.

[17] J. A. Kong. *Electromagnetic Wave Theory*. EMW, 2000.

[18] F. Ling and J. M. Jin. Scattering and radiation of microstrip antennas using discrete complex image method and reciprocity theorem. *Microwave & Optical Technology Lett.*, 16:212–216, 1997.

[19] Charles Van Loan. *Computational Frameworks for the Fast Fourier Transform*. Society for Industrial and Applied Mathematics, 1992.

[20] L. N. Medgyesi-Mitschang, J. M. Putnam, and M. B. Gedera. Generalized method om moments for three-dimensional penetrable scatterers. *J. Opt. Soc. Am. A*, 11(4):1383–1398, 1994.

[21] X. C. Nie, L. W. Li, and N. Yuan. Precorrected-FFT algorithm for solving combined field integral equations in electromagnetic scattering. *J. Electromagn. Waves Appl.*, 16(8):1171–1187, Aug. 2002.

[22] X. C. Nie, L. W. Li, N. Yuan, and T. S. Yeo. Fast analysis of scattering by arbitrarily shaped three-dimensional objects using the precorrected-FFT method. *Microwave Opt. Technol. Lett.*, 34(6):438–442, Sept. 2002.

[23] X. C. Nie, L. W. Li, N. Yuan, T. S. Yeo, and Y. B. Gan. A fast analysis of arbitrarily shaped homogeneous dielectric objects. *Microwave Opt. Technol. Lett.*, 38(1):30–34, July 2003.

[24] J. R. Phillips and J. K. White. A precorrected-FFT method for capacitance extraction of complicated 3-D structures. In *Proc. Int. Conf. Computer-Aided Design*, pages 268–271, Santa Clara, CA, 1994.

[25] J. R. Phillips and J. K. White. A precorrected-FFT method for electrostatic analysis of complicated 3-D structures. *IEEE Trans. Computer-Aided Design*, 16:1059–1072, Oct. 1997.

[26] M. A. Popovic, M. R. Watts, T. Barwicz, P. T. Rakich, L. Socci, E. P. Ippen, F. X. Kartner, and H. I. Smith. High-index-contrast, wide-FSR microring-resonator filter design and realization with frequency-shift compensation. In *Proceedings of Optical Fiber Communication Conf*, Washington DC, 2005.

[27] M. L. Povinelli, Steven G. Johnson, and J. D. Joannopoulos. Slow-light, band-edge waveguides for tunable time delays. *Optics Express*, 13(18):7145–7159, 2005.

[28] D. M. Pozar. Improved computational efficiency for the moment method solution of printed dipoles and patches. *Electromagn.*, 3:299–309, Sept. 1984.

[29] S. M. Rao, D. R.Wilton, and A.W. Glisson. Electromagnetic scattering by surfaces of arbitrary shape. *IEEE Trans. Antennas Propagat.*, 30:409–418, May 1982.

[30] Z. S. Sacks, D. M. Kingsland, R. Lee, and J. F. Lee. A perfectly matched anisotropic absorber for use as an absorbing boundary condition. *IEEE Trans. Antennas Propagat.*, 43(12):1460– 1463, 1995.

[31] J. J. Sakurai. *Modern Quantum Mechanics*. Addison-Wesley, 1994.

[32] D. H. Schaubert, D. R. Wilton, and A. W. Glisson. A tetrahedral modeling method for electromagnetic scattering by arbitrarily shaped inhomogeneous dielectric bodies. *IEEE Trans. Antennas Propagat.*, 32(1):77–85, 1984.

[33] Xing Qing Sheng, Jian-Ming Jin, Jiming Song, Weng Cho Chew, and Cai-Cheng Lu. Solution of combined-field integral equation using multilevel fast multipole algorithm for scattering by homogeneous bodies. *IEEE Trans. Antennas Propagat.*, 46(11):1718–1726, 1998.

[34] J. M. Song, C. C. Lu, and W. C. Chew. Multilevel fast multipole algorithm for electromagnetic scattering by large complex objects. *IEEE Trans. Antennas Propagat.*, 45(10):1488–1493, 1997.

[35] G. Strang. A proposal for Toeplitz matrix calculations. *Studies in Applied Mathematics*, 74:171–176, 1986.

[36] Allen Taflove. *Computational Electrodynamics: the Finite-difference Time-Domain Method*. Artech House, 1995.

[37] K. Umashankar, A. Taflove, and S. M. Rao. Electromagnetic scattering by arbitrary shaped three-dimensional homogeneneous lossy dielectric objects. *IEEE Trans. Antennas Propagat.*, 34(6):758–765, June 1986.

[38] C. F. Wang, F. Ling, and J. M. Jin. A fast full-wave analysis of scattering and radiation from large finite arrays of microstrip antennas. *IEEE Trans. Antennas Propagat.*, 46:1467–1474, Oct. 1998.

[39] A. J. Ward and J. B. Pendry. A program for calculating photonic band structures, Green's functions and transmission/reflection coefficients using a non-orthogonal FDTD method. *Comput. Phys. Comm.*, 128(3):590–621, 2000.

[40] J. Y. Wu, D. M. Kingsland, J. F. Lee, and R. Lee. A comparison of anisotropic PML to berenger's pml and its application to the finite-element method for EM scattering. *IEEE Trans. Antennas Propagat.*, 45(1):40– 50, 1997.

[41] K. L. Wu, M. Spenuk, J. Litva, and D. G. Fang. Theoretical and experimental study of feed network effects on the radiation pattern of series fed microstrip antenna arrays. *Proc. Inst. Elect. Eng.*, 138:238–242, June 1991.

[42] K. S. YEE. Numerical solution of initial boundary problems involving Maxwell's equations in isotropic media. *IEEE Trans. Antennas Propagat.*, 14:302–307, 1966.

[43] N. Yuan, T. S. Yeo, X. C. Nie, and L. W. Li. A fast analysis of scattering and radiation of large microstrip antenna arrays. *IEEE Trans. Antennas Propagat.*, 51(9):2218–2216, Sept. 2003.

[44] Lei Zhang, Ning Yuan, Min Zhang, L. W. Li, and Y. B. Gan. Rcs computation for a large array of waveguide slots with finite wall thickness using the mom accelerated by p-fft algorithm. *IEEE Trans. Antennas Propagat.*, 53(9):3101– 3105, 2005.

[45] Z. Zhu, B. Song, and J. White. Algorithms in fastimp: a fast and wideband impedance extraction program for complicated 3-D geometries. In *Proceedings of DAC*, pages 712–717, 2003.

[46] Y. Zhuang, K. L. Wu, C. Wu, and J. Litva. A combined full wave cgfft method for rigorous analysis of large microstrip antenna arrays. *IEEE Trans. Antennas Propagat.*, 44:102–109, Jan. 1996.